

The new field of nanopiezotronics

Semiconducting and piezoelectric nanowires and nanobelts have exciting applications in electronics, optoelectronics, sensors, and the biological sciences. We review the use of ZnO nanowires and nanobelts in electromechanical coupled devices. A nanogenerator that uses aligned ZnO nanowires for converting nanoscale mechanical energy into electric energy is described. The mechanism of the nanogenerator relies on the unique coupling of ZnO's piezoelectric and semiconducting properties. The approach has the potential to convert biological mechanical energy, acoustic/ultrasonic vibration energy, and biofluid hydraulic energy into electricity, demonstrating a new pathway for harvesting energy for self-powered wireless nanodevices and nanosystems. Based on the nanogenerator mechanism, we also describe piezoelectric field-effect transistors, diodes, force/pressure sensors, and resonators. These devices form the fundamental components of *nanopiezotronics*, a new field in nanotechnology.

Zhong Lin Wang

School of Materials Science and Engineering, Georgia Institute of Technology, Atlanta, GA 30332-0245, USA

E-mail: zhong.wang@mse.gatech.edu

Oxide nanomaterials have a great number of technological applications. Since the first synthesis of oxide nanobelts (NBs)¹ in 2001, research on functional oxide-based one-dimensional nanostructures has rapidly expanded because of their unique and novel applications in optics, optoelectronics, catalysis, and piezoelectricity. Semiconducting oxide NBs are a unique group of quasi-one-dimensional nanomaterials, which have been systematically studied for a wide range of materials with distinct chemical compositions and crystallographic structures².

Among transparent conducting oxides, ZnO is probably the most commonly studied material as it has the following unique merits. First, ZnO is a wide-bandgap semiconductor that has huge potential for electronic, optoelectronic, and optical applications. Second, it is unique in having semiconducting, piezoelectric, and pyroelectric properties, and is an ideal candidate for fabricating electromechanical coupled devices. Third, ZnO is a biodegradable and possibly biocompatible material suitable for medical and biological applications³. Fourth, ZnO nanostructures, such as dots, wires and belts, can be easily formed

using either a chemical approach at low temperature (70°C) or physical methods at high temperature (500–600°C) over a wide range of substrates. Finally, ZnO has O²⁻- and Zn²⁺-terminated surfaces (i.e. polar surfaces). The electrostatic interaction energy and distinct chemical activities of the polar surfaces results in the formation of a wide range of structures, such as nanosprings⁴, nanorings⁵, nanobows⁶, and nanohelices⁷, as reviewed previously^{8,9}. This review covers the novel devices and applications that have been demonstrated using piezoelectric nanowires (NWs) and NBs. A new field of nanopiezotronics is thus established.

Nanomanufacturing of aligned nanowires

Research in synthesizing semiconducting nanostructures is an area at the forefront of nanotechnology because of the applications in nanoelectronics, photonics, data storage, and sensing. Device arrays will require large-scale and controlled synthesis of nanostructures, and so it is essential to find experimental conditions under which the desired nanostructures can be synthesized reproducibly, in large quantities, and with controlled morphology. In nanopiezotronics, a key requirement is the synthesis of aligned arrays of NWs with controlled structures over large areas. This is an important step toward nanomanufacturing rather than fabrication of small numbers of nanoscale devices.

ZnO NWs have been grown on a solid-state or polymer substrate using Au¹⁰ and Sn¹¹ as catalysts. In the vapor-liquid-solid (VLS) growth method, the catalyst initiates and guides the growth and the epitaxial relationship between the NWs and the substrate leads to the aligned growth. We have combined a self-assembly based mask technique with the epitaxial approach to grow large-area hexagonal arrays of aligned ZnO NWs (Fig. 1a)^{12–14}.

A key requirement for nanopiezotronics is the reproducible synthesis of NWs over a large surface area at high yield. In VLS growth, it may be assumed that NWs grow as long as catalysts are supplied and the temperature is adequate. However, we have shown that oxygen partial pressure in the chamber plays a key role in determining the quality of the aligned ZnO NWs. A 'phase diagram' has been derived for oxygen partial pressure and growth chamber pressure in synthesizing high-quality, aligned ZnO NWs on a GaN substrate (Fig. 1b)¹⁵. NWs only grow under the conditions defined by the red zone in the plot. This result provides a roadmap for large-scale, controlled synthesis of aligned ZnO NWs with the potential to meet the needs of practical applications.

We have also explored how we can control the high-yield synthesis of CdSe NWs, NBs, or nanosaws by systematically investigating the effect of experimental conditions¹⁶. CdSe exhibits one-dimensional nanostructure morphologies of NWs, NBs, and nanosaws (Figs. 1c–e), but it is unfortunate that the as-synthesized nanostructures are a mixture of the three¹⁷. It is desirable to control the purity of the as-synthesized CdSe nanostructures so that we can obtain a specific morphology at close to 100% yield. To investigate the relationship

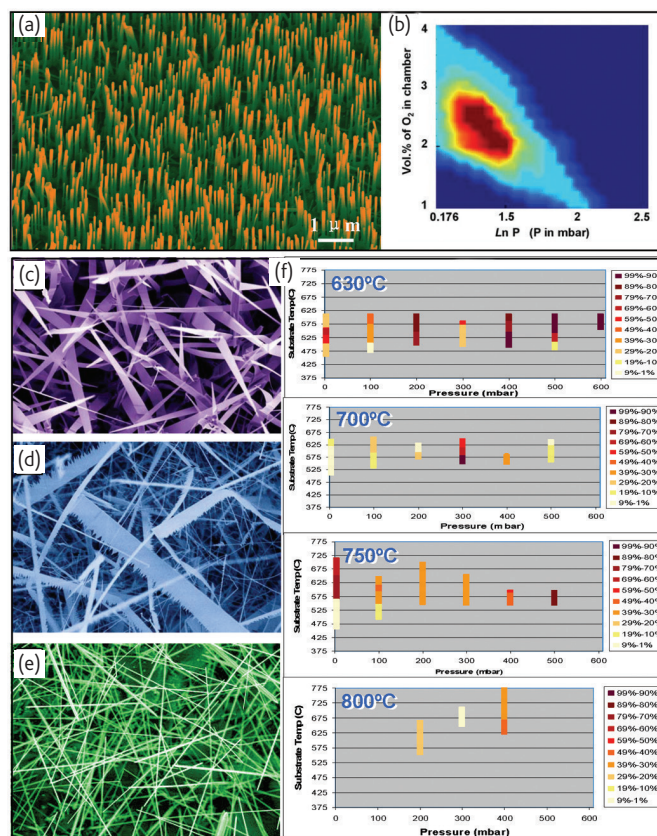


Fig. 1 'Phase diagram' and 'roadmap' for synthesis of NWs and NBs. (a) Aligned ZnO NWs grown on a single-crystal alumina substrate with a honeycomb pattern defined by the catalyst mask. (b) 'Phase diagram' showing the effect of oxygen partial pressure and total pressure in the growth chamber on the growth of ZnO NWs. (c) NBs, (d) nanosaws, and (e) NWs of CdSe. (f) Yield of CdSe nanosaws as a function of chamber pressure at four different furnace temperatures. The strength of the color indicates the percentage yield of the product^{12,15,16}.

between morphology, temperature, and pressure in the growth of this material, the source temperature of the system was held constant while the pressure was held at one of nine set values: 800 mbar, 700 mbar, 600 mbar, 500 mbar, 400 mbar, 300 mbar, 200 mbar, 100 mbar, and 4 mbar. This was repeated at five different source temperatures: 850°C, 800°C, 750°C, 700°C, and 630°C, giving a total of 45 distinct datasets. This has allowed a 'roadmap' for guiding CdSe synthesis to be defined¹⁶.

The source temperature stimulates the vaporization of the source materials, and the subsequent growth is controlled predominantly by the local temperature and pressure at the substrate. There is an increase in the growth temperature range where deposition occurs with a decrease in the system pressure. A lower source temperature than normal for synthesis of 630°C, a high chamber pressure (600 mbar), and 575 ± 5°C substrate temperature produces the highest percentage of nanosaws/nanocombs (Fig. 1f). A source temperature of 700°C, a low chamber pressure (4 mbar), and substrate temperature of

$575 \pm 8^\circ\text{C}$ produces the highest percentage of NBs. Growth of NWs is less restrictive and it can be carried out over a wide range of temperature and pressure.

Future nanomanufacturing requires controlled, rationally designed, and large-scale synthesis of nanomaterials. The first step is to determine the phase diagrams and roadmaps for the synthesis of nanomaterials. To meet this goal, a substantial amount of work is required to improve and optimize our current approaches in nanomaterials synthesis. An alternative is to use statistical modeling for guiding synthesis. Recently, statistical analysis techniques have been applied for the first time for modeling and optimizing the experimental parameters required for synthesizing desired nanostructures¹⁸. This pioneering work uses finite experimental data to predict the optimum experimental conditions for achieving desired nanostructures.

Piezoelectric nanogenerators

Wireless devices may allow *in situ*, real-time biomedical monitoring, but such devices still require a power source. Ideally, such devices should be self-powered rather than use a battery. The body provides numerous potential energy sources – mechanical energy, vibrational energy, chemical energy, and hydraulic energy – but their efficient conversion into electric energy is a challenge. If this can be accomplished on the nanoscale, such power sources could greatly reduce the size of integrated nanosystems for optoelectronics¹⁹, biosensors²⁰,

resonators²¹, etc. We have demonstrated an approach that converts mechanical energy into electric power using aligned ZnO NWs²².

Our work is based on aligned ZnO NWs grown on a c-plane oriented $\alpha\text{-Al}_2\text{O}_3$ substrate covered by a layer of ZnO film (Fig. 2a). Atomic force microscopy (AFM) measurements were performed using a Si tip coated with Pt film. In contact-mode AFM, a constant normal force of 5 nN was maintained between the tip and sample surface. The tip is scanned over the top of the ZnO NW, and its height adjusted according to the surface morphology and local contact force. The output voltage across an outside load of resistance $R_L = 500 \text{ M}\Omega$ was monitored continuously as the tip is scanned over the NWs (Fig. 2b; note the polarity of the voltage signal). No external voltage was applied at any stage of the experiment.

Images of both the topography (feedback signal from the scanner) and the corresponding output voltage (V_L) across the load were recorded simultaneously as the AFM tip was scanned over the NW arrays. In the voltage output images, many sharp output peaks (like discharge peaks) are observed. They are typically about 4–50 times higher than the noise level (Fig. 2c). The locations of the voltage peaks are directly registered at the sites of the NWs.

The physical principle for creating, separating, and preserving piezoelectric charges in the NWs is a coupling of piezoelectric and semiconducting properties²³. For a vertical, straight ZnO NW (Fig. 3a), the deflection of the NW by the AFM tip creates a strain field, with the

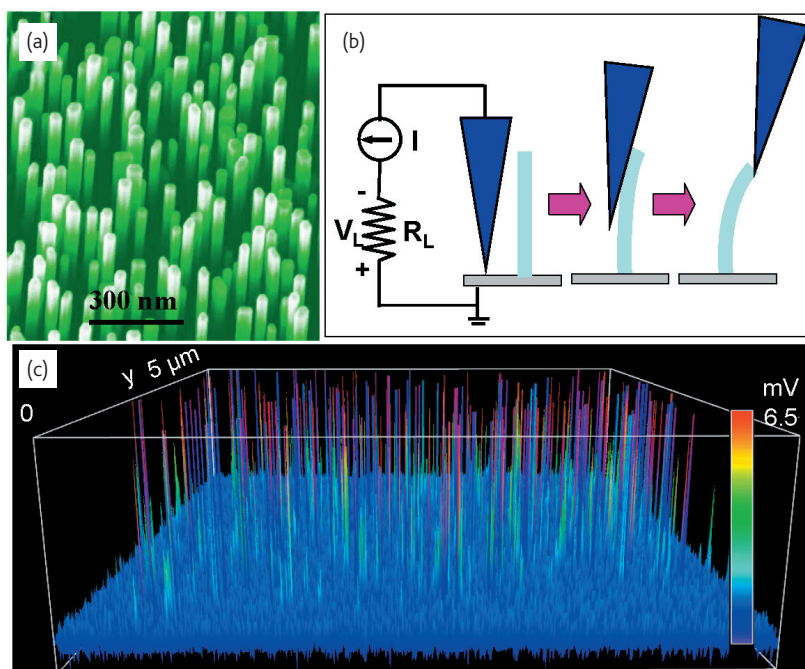


Fig. 2 (a) Scanning electron microscopy (SEM) images of aligned ZnO NWs grown on an $\alpha\text{-Al}_2\text{O}_3$ substrate. (b) Experimental setup for generating electricity through the deformation of a semiconducting and piezoelectric NW using a conductive AFM tip. The root of the NW is grounded and an external load of $R_L = 500 \text{ M}\Omega$ is applied, which is much larger than the inner resistance R_i of the NW. The AFM tip is scanned across the NW array in contact mode. (c) Output voltage image obtained when the AFM tip scans across the NW array. The discharging process is so quick that each discharge event is characterized by only a couple of data points^{22,23}.

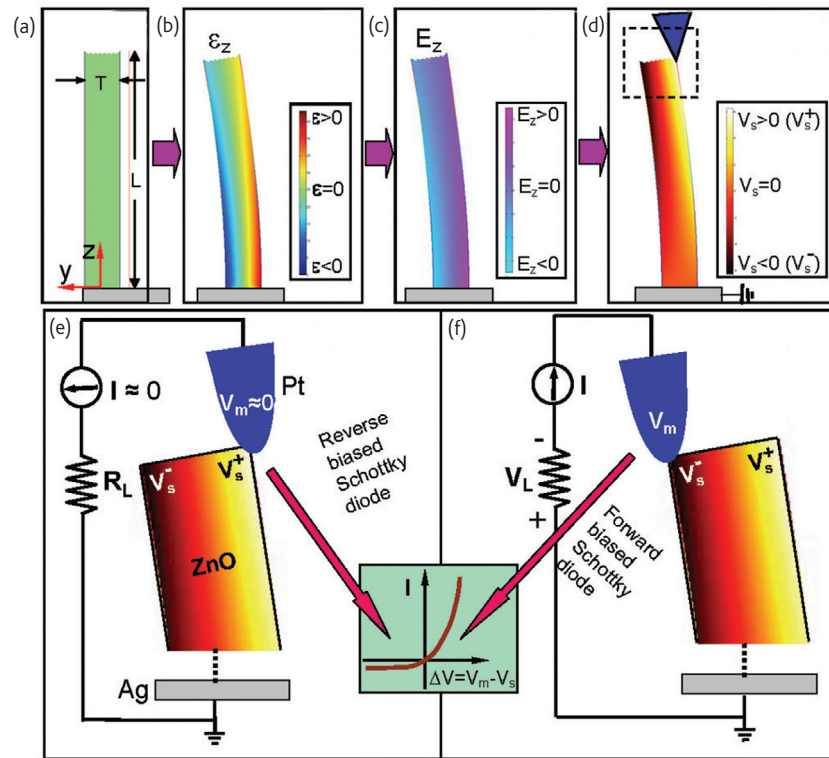


Fig. 3 Principle of power generation in a ZnO NW. (a) Schematic of the NW and coordinate system. (b) Longitudinal strain ϵ_z distribution in the NW after deflection by an AFM tip from the side. Image shows a FEMLAB simulation for a ZnO NW of length $1\ \mu\text{m}$ and aspect ratio of 10. (c) Corresponding longitudinal electric field E_z distribution in the NW induced by the piezoelectric effect. (d) Potential distribution in the NW. The dashed box indicates the area shown in parts (e) and (f). (e), (f) Interface between the metal AFM tip and semiconducting ZnO NW under local positive and negative contact potentials, showing reverse- and forward-biased Schottky rectifying behavior, respectively. This oppositely biased Schottky barrier across the NW makes it possible to preserve the piezoelectric charges and produce a voltage discharge output. Inset: typical I - V characteristic of a metal-semiconductor (n -type) Schottky barrier. The process in (e) builds up the potential; the process in (f) discharges the potential^{22,23}.

outer surface being stretched (positive strain ϵ) and the inner surface compressed (negative strain $-\epsilon$) (Fig. 3b). An electric field E_z along the NW (z direction) is then created inside the NW volume through the piezoelectric effect, $E_z = \epsilon_z/d$, where d is the piezoelectric coefficient²⁴ along the NW direction (normally the positive c -axis of ZnO, with the Zn atomic layer being the front terminating layer²⁵). The piezoelectric field direction is closely parallel to the z -axis (NW direction) at the outer surface and antiparallel to the z -axis at the inner surface (Fig. 3c). Across the top of the NW, to a first-order approximation, the electric potential distribution varies from V_s^- (negative) at the compressed side to V_s^+ (positive) at the stretched surface. The electrode at the base of the NW is grounded.

Note that V_s^+ and V_s^- are voltages produced by the piezoelectric effect. The potential is created by the relative displacement of the Zn^{2+} cations with respect to the O^{2-} anions through the piezoelectric effect in the wurtzite crystal structure. Thus, these ionic charges cannot move freely or recombine without releasing the strain (Fig. 3d). The potential difference is maintained as long as the deformation remains and no foreign free charges (such as from the metal contacts) are injected.

We now consider the discharge process. The conductive AFM tip that induces the NW deformation is initially in contact with the stretched NW surface of positive potential V_s^+ (Figs. 3d, 3e). The Pt metal AFM tip has a potential of nearly zero, $V_m = 0$, so the Pt-ZnO interface is negatively biased: $\Delta V = V_m - V_s^+ < 0$. Since as-synthesized ZnO NWs are n -type, the Pt metal-ZnO semiconductor (M-S) interface is a reverse-biased Schottky diode and little current flows across the interface (Fig. 3e). When the AFM tip is in contact with the compressed side of the NW (Fig. 3f), the tip-NW interface is positively biased, $\Delta V = V_m - V_s^- > 0$. The M-S interface is a positively biased Schottky diode, and there is a sudden increase in the output electric current. The current is the result of the ΔV -driven flow of electrons from the semiconducting ZnO NW to the metal AFM tip. The flow of the free electrons from the loop through the NW to the tip will neutralize the ionic charges distributed in the volume of the NW, and thus reduce the magnitudes of the potentials V_s^+ and V_s^- . The principle demonstrated in Fig. 3 is the basis of *nanopiezotronics*.

This technology has the potential to convert mechanical energy (such as body movement, muscle stretching, blood pressure), vibration

energy (such as acoustic/ultrasonic waves), and hydraulic energy (such as blood flow, contraction of blood vessels, dynamic fluids in nature) into electrical energy, and may be sufficient for powering nanodevices and nanosystems. The technology could have important applications in wireless, self-powered nanodevices by harvesting energy from the environment. It also provides a method for indirect charging of a battery. High power output electric generators could be fabricated by using arrays of ZnO wires/belts, which could be grown on substrates such as metal foils, flexible plastics²⁶, ceramics such as alumina, and compound semiconductors such as GaN and AlN. These nanogenerators could be the basis for exploring new self-powered technologies for *in situ*, real-time, and implantable biosensing, biomedical monitoring, and biodetection.

Flexible power generator built on a polymer substrate

The ceramic or semiconductor substrates used for growing ZnO NWs are hard, brittle, and could be used in areas that require a foldable or flexible power source²⁷, such as implanted biosensors in muscles or joints, or power generators built into shoes. It is necessary instead to use conductive polymer/plastics as substrates that are also likely to be biocompatible and biodegradable. Two advantages are offered by this approach. One is that the large-scale solution method used to grow ZnO NW arrays at a temperature <80°C would be more cost effective. The other is the large choice of available flexible plastic substrates for growing aligned ZnO NW arrays.

Highly aligned ZnO NWs have been grown using chemical synthesis. Figs. 4a and 4b show optical and scanning electron microscopy (SEM) images of ZnO NW arrays grown on a conductive plastic substrate, which can be rather large on the order of 10-100 cm². Using a patterned Au catalyst, the density and distribution of the NWs can be controlled according to a predetermined design (Fig. 4c). Various dimensions, shapes, and orientations of NWs have been grown at low temperature in this way. To improve the adhesion of NWs on the substrate, a thin layer of polymer can be spun onto the substrate after growth, so that the roots of the NWs are partially embedded (Fig. 4d). Electrical energy can be generated using the setup shown in Fig. 2, and an output of ~20 mV has been achieved (Fig. 4e). Piezoelectric power generators using ZnO NW arrays on flexible plastic substrate might be able to harvest energy from the environment, relying on body movement, for example, in the form of gestures, respiration, or locomotion.

Piezoelectric field-effect transistor

Field-effect transistors (FETs) based on NWs and nanotubes are some of the most frequently studied nanodevices. A typical NW FET is composed of a semiconducting NW connected at the ends by two electrodes and placed on a Si substrate covered by a thin layer of oxide. The Si substrate can be used as the gate electrode or a third electrode

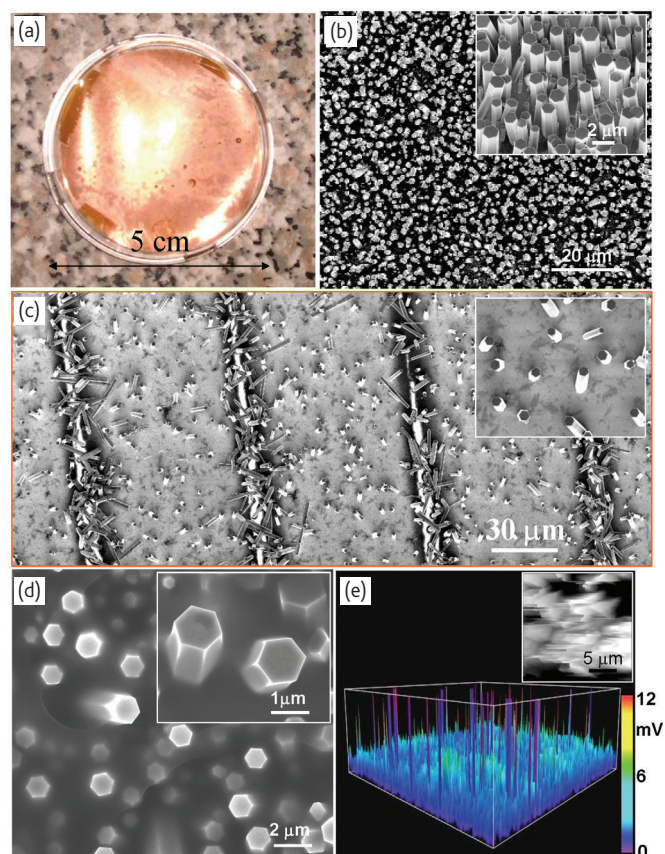


Fig. 4 (a) Optical image of aligned ZnO NWs grown on a polymer substrate. (b) SEM image of ZnO NWs synthesized using a chemical approach. (c) SEM image of ZnO NWs grown on a patterned substrate. (d) Top view SEM image showing aligned ZnO wires on a plastic substrate coated with poly(methyl methacrylate), or PMMA, for reinforcement. Inset: enlarged view of the PMMA-encapsulated microwires. (e) Corresponding voltage output profile under AFM measurement. Inset: topography image of the 20 μm x 20 μm area²⁷.

can be built on the top or bottom of the NW. The signal output from the drain electrode of the NW is controlled by a gate voltage applied between the gate and the NW.

A sensor can be fabricated from a source-drain structured NW FET without a gate. Thus, a large portion of the NW is exposed to the environment. The mechanism for sensing gases, biomolecules, and even viruses relies on the creation of a charge depletion zone in the semiconductor NW by surface-adsorbed targets¹⁷.

By connecting a ZnO NW across two electrodes that can apply a bending force to the NW, the piezoelectric field created across the bent NW serves as the gate for controlling the electric current flowing through the NW²⁸. This piezoelectric FET can be considered as a new type of transistor that is turned on/off by applying a mechanical force. As a result, it can act as a force sensor capable of measuring forces in the nanoNewton range and smaller.

The experimental setup is shown in Fig. 5a. W metal electrodes form ohmic contacts with the ZnO NW. A force is applied to one of the movable electrodes by an external piezoelectric actuator, bending

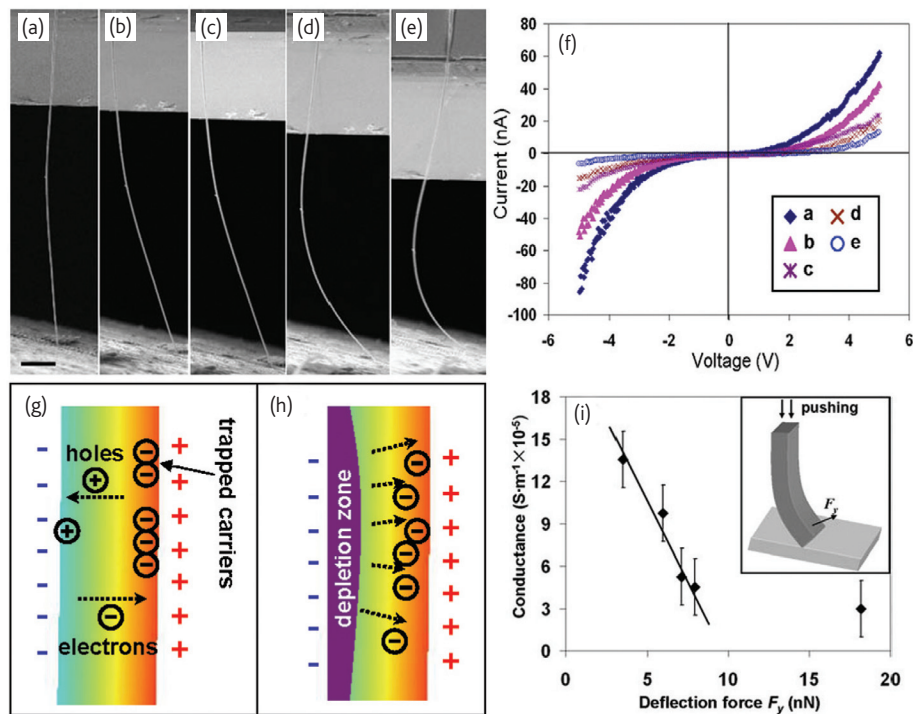


Fig. 5 (a–e) SEM images showing five different examples of bends introduced into a ZnO NW. Scale bar = 10 μm . (f) Corresponding I - V characteristics of the ZnO NW for the five different bending cases. Schematics showing the mechanisms responsible to the conductance change: (g) the carrier trapping effect; and (h) the creation of a charge depletion zone. (i) Plot showing the relationship between the ZnO NW conductance and the deflection force derived from the experimental data, demonstrating a nanoscale force or pressure sensor using a single NW. Inset: schematic of the deflected NW²⁸.

the NW. During this process, the I - V characteristics of the device are monitored continuously. Five typical bending curvatures of the ZnO NW are shown in SEM images in Figs. 5a–e, and their corresponding I - V curves are presented in Fig. 5f. The symmetric shape of the I - V curves indicates good ohmic contacts at both ends of the NW¹⁹. The current drops significantly with increased bending (curves b–e in Fig. 5f), indicating decreased conductance with increased strain.

A possible mechanism has been proposed to explain the observed phenomenon²⁸. First, it is worth examining the coupling between the piezoelectric and semiconducting properties. In 1970, a 75% decrease in in-plane conductance of a semiconducting Si slab was observed when it was sandwiched between two pieces of piezoelectric lead-zirconium-titania (PZT) crystal and the assembly excited by application of an ac signal across its cross section²⁹. The drop in Si conductance in the direction orthogonal to the propagation of the elastic wave in PZT was attributed to the trapping of free carriers at the surfaces of the Si plate. This is a result of coupling between the semiconductor Si crystal and the PZT piezoelectric crystal. The coupling effect can now be achieved in a single ZnO NW because of its dual semiconducting and piezoelectric properties.

As shown in Fig. 2, a bent ZnO NW can have positively and negatively charged surfaces at the outer and inner bending arcs of the

NW, respectively, because of the stretching and compression of the surfaces⁸. The charges are induced by the piezoelectric effect and are static and nonmobile ionic charges. Upon build up of the electric field, two possible effects can be proposed to account for the reduction of the NW conductance: a carrier trapping effect and the creation of a charge depletion zone.

When a piezo-potential is induced across a bent NW, some free electrons in the n -type ZnO NW may be trapped at the positive, outer surface, thus lowering the effective carrier density in the NW (Fig. 5g). Although the positive potential could be partially neutralized by the trapped electrons, the negative potential would remain unchanged. Hence, the piezoelectric field is retained across the width of the NW. This situation can be compared to the case of applying a gate voltage across the diameter of the ZnO NW, as in a typical NW FET. Free electrons will be repelled by the negative potential and form a charge depletion zone around the compressed side, as shown in Fig. 5h. Consequently, with NW bending, the width of the conducting channel in the ZnO NW becomes smaller and smaller, while the depletion region becomes larger and larger. The depletion zone can develop up to the strain-free plane as a maximum (close to central axis of the NW), considering the piezoelectric field that naturally sets an upper limit to the effect contributed by the depletion charges. The two effects

presented in Figs. 5g and 5h are likely to contribute to the dramatic drop in the conductance of the ZnO NW with an increase in bending.

Based on the principle of the piezoelectric FET, a nanoscale force/pressure sensor can be demonstrated. The mechanical force applied to the NW can be determined from its bent shape. Thus, a force sensor is established that can measure tiny forces in the nanoNewton range (Fig. 5i)²⁸.

Piezoelectric-gated diode

A piezoelectric-gated diode has been demonstrated using a two-probe technique³⁰. Fig. 6a illustrates a manipulator making a two-terminal connection to a single ZnO NW to measure its electrical transport properties. The difference between this experimental setup and the piezoelectric FET is that only one side of the bent NW is in contact with the probe. One probe holds the NW stationary, while the other bends the NW from the tensile side. A typical sequence of images of the ZnO NW bent at various angles with the corresponding I - V curves are shown in Figs. 6b-e. When the Ti-coated tip first contacts the NW (Fig. 6b), the linear and symmetric I - V characteristics show that the contact is an ohmic one and not a double (back-to-back) Schottky

contact. As the bending proceeds (Figs. 6c-e), the current drops significantly for negative bias, exhibiting an asymmetric I - V behavior with increased strain. It can be clearly seen that the probe is firmly attached to the NW and shows no sliding, indicating the contacts are retained during the bending process without any change in contact resistance or contact area. The reverse current drops significantly under reverse bias voltage when the NW is bent further. Under severe bending, the reverse current at a bias of -5 V can be as low as $\sim 6.6 \mu\text{A}$ and the rectifying ratio at ± 5 V is up to 8.7:1. Because of the large elasticity of the NW, the devices are reversible.

The observed diode effect may be explained using the mechanism illustrated in Fig. 3³⁰. We assume that before bending, there is no energy barrier but a contact resistance between the Ti tip and the ZnO NW. When the probe pushes the NW and bends it, a positive potential is produced at the stretched side of the NW because of the piezoelectric effect. As a result, an energy barrier is produced at the interface between the tip and the NW, with the NW being at a higher potential (Figs. 6f and 6g). Note that the actual potential distribution is not fixed because of the nonuniform distribution of strain. For the bent ZnO NW under forward bias, the electrons are

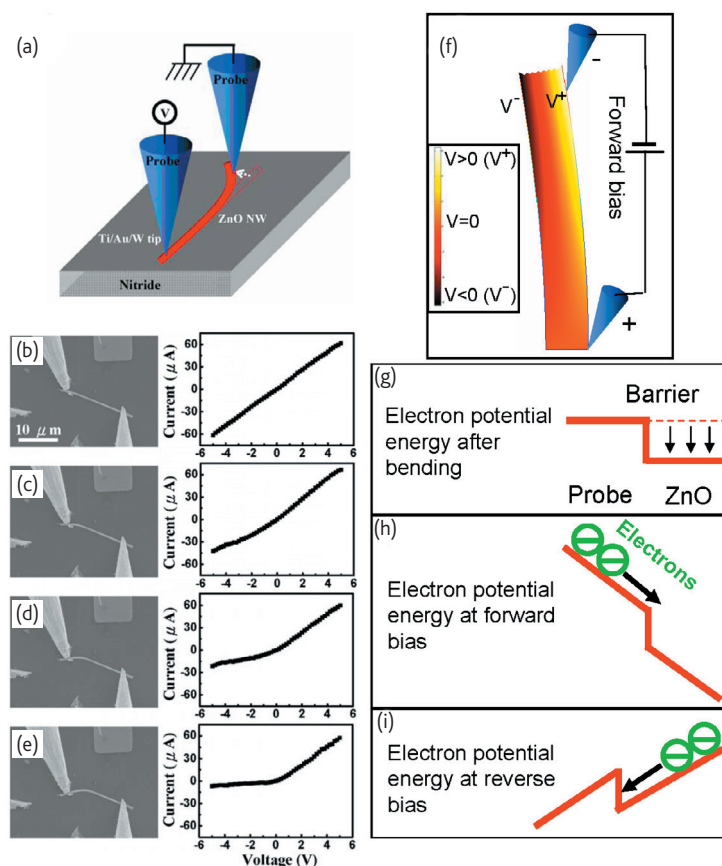


Fig. 6 (a) Schematic of the nanomanipulation and in situ I - V measurement system. (b-e) Sequence of SEM images of the ZnO NW at various bending angles and the corresponding I - V characteristics. (f) Piezoelectric potential distribution in a bent NW. (g) Energy barrier formed at the probe tip-NW interface as a result of the piezoelectric potential (V^+) at the stretched side. (h) Current flow under forward bias. (i) Current flow under reverse bias³⁰.

not blocked by this energy barrier (Fig. 6h). On the other hand, under reverse bias, electrons need to overcome this barrier (Fig. 6i). This energy diagram corresponds well to the observed electric transport measurements on bent ZnO NWs. The energy barrier effectively serves as a p - n junction at the tip-NW interface, which resists current flow from the tip to the NW, but current can flow from the NW to the tip. The magnitude of the barrier increases with the degree of bending, resulting in an enhanced rectifying effect. This is a piezoelectric-gated diode.

Piezoelectric resonator

Bulk acoustic resonators (BARs) are important devices for communication systems. They consist of a thin piezoelectric film sandwiched between two electrodes. A radio-frequency signal applied across the thickness of the film produces mechanical motion, and the fundamental resonance occurs when the film thickness equals half of the wavelength of the input signal.

Piezoelectric ZnO NBs can be effective piezoelectric resonators because of their high uniformity and dislocation-free structure. Using a single belt, we have demonstrated a BAR (Fig. 7a)⁶. By measuring the impedance response across the NB (Fig. 7b), the resonance frequency can be identified in both the phase and amplitude traces (Fig. 7c). The fabricated device was characterized using vector network analysis, and the first and third harmonics were observed at approximately 247 MHz and 754 MHz, respectively. A one-dimensional Krimholt-Leedom-Matthaei (KLM) model was used to predict the resonant frequency of the device and confirm the observed behavior (Fig. 7c).

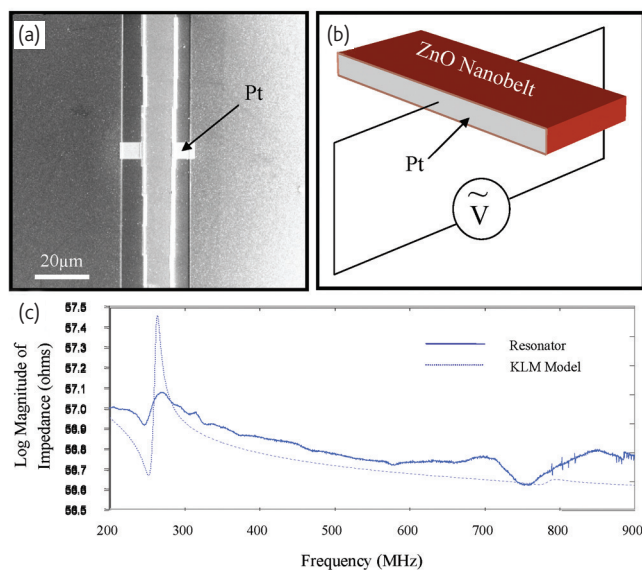


Fig. 7 (a) SEM image of a ZnO NB resonator. The ZnO NB is in the center, sandwiched by two Pt electrodes that are connected to an external ac circuit. (b) Schematic of the piezoelectric resonator design. (c) Plot of magnitude $|Z|$ of the measured impedance across the NB as a function of the applied ac frequency. The predicted trace using the KLM model is also shown⁶.

Nanopiezotronics – a new field of research and applications

In piezoelectric applications, PZT ceramics are probably the preferred choice as far as performance is concerned. In comparison, nanopiezotronics using NWs/NBs as the fundamental building blocks has the following unique advantages. First, the NW-based nanogenerators can be subjected to extremely large deformations, so that they can be used in flexible electronics as a power source. Secondly, the large deformations that the NWs can withstand is likely to give a much larger power volume density output. Third, in contrast to PZT, ZnO is thought to be biocompatible and so has profound potential for power sources that are implantable into the human body. Fourth, the flexibility of the polymer substrate used for growing ZnO NWs makes it feasible for them to be accommodated within human muscles, so that the mechanical energy inherent in body movement and muscle stretching can be used to generate electricity. Fifth, ZnO nanogenerators can produce current directly because of ZnO's enhanced conductivity with the presence of oxygen vacancies. Finally, ZnO is a more environmental friendly material than PZT.

Based on coupling the semiconducting and piezoelectric properties of ZnO, we have explained the mechanism of the piezoelectric nanogenerator (Fig. 3). We have demonstrated piezoelectric FETs, diodes, and force/pressure sensors. These devices can be used as fundamental components in novel, nanoscale piezoelectronic systems. We call this *nanopiezotronics*, a new field of research and applications in nanotechnology³¹.

Superelasticity and fracture mechanics at the nanoscale

Once an object becomes small, its mechanical behavior can become drastically different. In nanopiezotronics, it is important to understand the deformation and fracture behavior of piezoelectric nanostructures.

It is generally known that bulk ceramics have little elasticity, but nanosized ceramic structures can be very different. Recently, superelasticity (a shape-memory behavior) has been discovered in superlattice-structured ZnO nanohelices^{7,26}. After manipulation using a nanoprobe, the nanohelix can elastically recover its shape after an extremely large axial stretching to a degree close to the theoretical limit (Figs. 8a-c), while suffering little residual plastic deformation. As a result, the spring constant of ZnO nanohelices can be continuously increased up to 300-800%. A shape memory/recovery effect has been observed after subjecting the nanohelix to a buckling deformation.

An AFM tip was used to compress a nanohelix in the transverse direction until fracture occurred²⁶. Fig. 8d is an SEM image of a nanohelix fractured by the AFM tip. Force-displacement curves for a group of nanohelices are shown in Fig. 8e. A common feature is that the force-displacement curve shows two sharp drops at F_1 and F_2 , the values of which depend on the size of the nanohelix. Complete fracture of the nanohelix follows a sharp drop at F_2 . A two-step mechanism

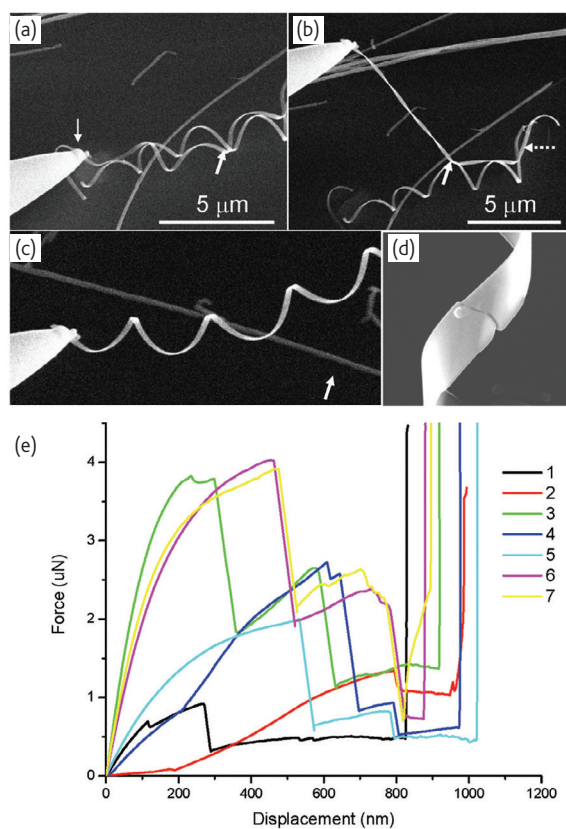



Fig. 8 A ZnO nanohelix shows an extremely large axial stretching followed by a shape recovery process. (a) One end of a nanohelix is welded with Pt onto a W nanoprobe. (b) Enlarged SEM image showing the stretched nanohelix. (c) Continued extraction leads to an initial release of the welded nanohelix from the entangled cluster and a recovery of the nanohelix shape. (d) SEM image of a nanohelix after fracture. The arrowheads indicate the points where the nanohelix was 'welded' to the nanoprobe. (e) Force-displacement curves for seven nanohelices recorded during AFM tip compression and fracture³¹.

could explain the force-displacement curves. We suggest that the first drop in force is a stretching of the nanohelix that induces a local buckling deformation. Once this occurs, the nanohelix becomes very soft. The second drop in force is likely to be related directly to the occurrence of fracture. The ZnO nanohelices may be of great interest for investigating nanoscale fracture processes.

Future perspectives

Nanodevices using piezoelectric NWs and NBs and their novel applications have been presented in this review. The future of nanotechnology research will move from single devices to the fabrication of arrays of devices with multifunctionality, then to integrated nanosystems. It is crucial to find various approaches that can feasibly harvest energy from the environment to self-power such nanosystems, so that they can operate wirelessly, remotely, and independently with a sustainable energy supply. The principle demonstrated in the piezoelectric nanogenerator could be the foundation for such self-powered nanosystems.

Based on the mechanism of the nanogenerator, several important prototype piezoelectric devices have been demonstrated, such as FETs, diodes, force/pressure sensors, and resonators. These devices are the fundamental components of *nanopiezotronics*, a new field in nanotechnology³¹. 

Acknowledgments

Thanks to Y. Ding, P. X. Gao, J. H. Song, X. D. Wang, R. S. Yang, C. S. Lao, J. H. He, Y. L. Chueh, L. J. Chou, L. J. Chen, W. L. Hughes, B. Buchine, C. J. Summers, W. J. Mai, J. Liu, D. Moore, N. S. Xu, C. Ma, and Y. F. Gao for their contributions to the work reviewed in this article. We acknowledge generous support from Defense Advanced Research Projects Agency, National Science Foundation, National Aeronautics and Space Agency, and the National Institutes of Health.

REFERENCES

- Pan, Z. W., et al., *Science* (2001) **291**, 1947
- Wang, Z. L., *J. Phys: Condens. Matter* (2004) **16**, R829
- Zhou, J., et al., *Adv. Mater.* (2006) **18**, 2432
- Kong, X. Y., and Wang, Z. L., *Nano Lett.* (2003) **3**, 1625
- Kong, X. Y., et al., *Science* (2004) **303**, 1348
- Buchine, B. A. et al., *Nano Lett.* (2006) **6**, 1155
- Gao, P. X., et al., *Science* (2005) **309**, 1700
- Wang, Z. L., *Materials Today* (2004) **7** (6), 26
- Wang, Z. L., et al., *Adv. Funct. Mater.* (2004) **14**, 944
- Yang, P. D., et al., *Adv. Funct. Mater.* (2002) **12**, 323
- Gao, P. X., et al., *Nano Lett.* (2003) **3**, 1315
- Wang, X. D., et al., *Nano Lett.* (2004) **4**, 423
- Wang, X. D., et al., *J. Phys. Chem. B* (2006) **110**, 7720
- Wang, X. D., et al., *J. Am. Chem. Soc.* (2005) **127**, 7920
- Song, J. H., et al., *J. Phys. Chem. B* (2005) **109**, 9869
- Ma, C., and Wang, Z. L., *Adv. Mater.* (2005) **17**, 2635
- Ma, C., et al., *J. Am. Chem. Soc.*, (2004) **126**, 708
- Dasgupta, T., et al., *J. Am. Stat. Assoc.* (2007), in press
- Duan, X. F., et al., *Nature* (2003) **421**, 241
- Zheng, G. F., et al., *Nat. Biotechnol.* (2005) **23**, 1294
- Bai, X. D., et al., *Appl. Phys. Lett.* (2003) **82**, 4806
- Wang, Z. L., and Song, J. H., *Science* (2006) **312**, 242
- Song, J. H., et al., *Nano Lett.* (2006) **6**, 1656
- Zhao, M. H., et al., *Nano Lett.* (2004) **4**, 587
- Wang, Z. L., et al., *Phys. Rev. Lett.* (2003) **91**, 185502
- Gao, P. X., et al., *Nano Lett.* (2006) **6**, 2536
- Gao, P. X., et al., *Adv. Mater.* (2007) **19**, 67
- Wang, X. D., et al., *Nano Lett.* (2006) **6**, 2768
- Fischler, C., et al., *Appl. Phys. Lett.* (1970) **17**, 252
- He, Jr, H., et al., *Adv. Mater.* (2007), in press
- Wang, Z. L., *Adv. Mater.* (2007) **19**, 889